PHYSICAL REVIEW B **92**, 104101 (2015)

Interband transitions in epitaxial ferroelectric films of $NaNbO_3$

M. Tyunina,[1,2,*] D. Chvostova,[2] L. D. Yao,[3] A. Dejneka,[2] T. Kocourek,[2] M. Jelinek,[2] and S. van Dijken[3]
[1]*Microelectronics and Materials Physics Laboratories, University of Oulu, P.O. Box 4500, FI-90014 Oulun Yliopisto, Finland*
[2]*Institute of Physics, Academy of Sciences of the Czech Republic, Na Slovance 2, 182 21 Prague 8, Czech Republic*
[3]*NanoSpin, Department of Applied Physics, Aalto University School of Science, P.O. Box 15100, FI-00076 Aalto, Finland*
(Received 8 January 2015; revised manuscript received 2 March 2015; published 2 September 2015)

The interband optical transitions in cube-on-cube-type epitaxial ferroelectric $NaNbO_3$ thin films and a reference antiferroelectric $NaNbO_3$ crystal are studied in the spectral range of 0.74–9 eV using variable-angle spectroscopic ellipsometry. The energies and the types of the transitions in the films are found to differ significantly from those in the crystal and to vary with epitaxial strain. The results are discussed in terms of epitaxial effects, including higher crystal symmetry, anisotropic lattice strain, and ferroelectric polarization in the $NaNbO_3$ films compared to the crystal.

DOI: 10.1103/PhysRevB.92.104101 PACS number(s): 77.55.Px

I. INTRODUCTION

Perovskite-structure oxide ferroelectric crystals have long been used in optical and optoelectronic devices owing to their high transparency and large index of refraction in the visible range, excellent nonlinear optical properties, and high dielectric susceptibility. Advanced integrated photonic and optoelectronic applications require high-quality small-sized ferroelectrics, which can be achieved by the use of epitaxial ferroelectric thin films [1]. A number of photovoltaic, optoelectronic, and plasmonic devices using epitaxial ferroelectric films have already been demonstrated [2–5]. In order to fully employ the potential of such films, it is important to understand how epitaxy-related effects alter the optical properties of ferroelectric oxides.

Epitaxial growth of thin films on dissimilar substrates may result in the formation of new structural phases, produce significant lattice strains, and lead to the emergence of electronic and optical properties that do not exist in bulk crystals. In particular, epitaxial strain has been shown to reduce bandgaps in semiconductors, nonpolar metal oxides, and perovskite-type paraelectrics [6–8] and to result in complicated bandgap behavior in ferroelectrics [8,9]. However, the influence of crystal symmetry and lattice strain on the optical properties of heteroepitaxial ferroelectric thin films is not well understood yet.

As known from semiconductor physics, the optical properties are determined by interband electronic transitions, which can be related to Van Hove singularities in the joint density of states (DOS). In turn, the singularities in the DOS are connected to critical points (CPs) in the band structure, which describes the allowed energy states (valence and conduction bands) in momentum space. A theoretical model of CPs in a parabolic band approximation allows for accurate extraction of CP energies from experimental optical dielectric functions in semiconductors [10,11] and also in perovskite oxide ferroelectrics [12–14]. By comparing the experimentally determined energies with band-structure calculations, it is possible to assign CPs to specific points in the Brillouin zone (BZ) and thus to verify theory. The assignment of CPs in oxide ferroelectrics, however, has been difficult. More extensive experimental studies of interband transitions are therefore vital not only for a better knowledge and understanding of optical properties but also for the development of more extensive theory of ferroelectrics. Also it should be stressed that interband transitions determine optical refraction and electro-optic coefficients in ferroelectrics. Controlling these transitions by epitaxial growth can enable new optical materials and applications. Studies of interband transitions in epitaxial ferroelectric films are therefore of practical importance for emerging thin-film photonic and optoelectronic devices.

Here, we experimentally investigate effects of epitaxy on the optical properties of NaNbO3 (NNO). We apply CP analysis in order to quantify the changes of the interband transitions in epitaxial NNO films as a function of lattice strain and compare the transitions to those of a NNO reference crystal.

II. EXPERIMENT

Epitaxial perovskite $NaNbO_3$ films with thicknesses of 9–14 nm were selected for this study. The films were grown onto $(La_{0.18}Sr_{0.82})(Al_{0.59}Ta_{0.41})O_3$ (LSAT) (001), $SrTiO_3$ (STO) (001), MgO (001), and $DyScO_3$ (DSO) (011) single-crystal substrates (LSAT, STO, MgO, and DSO for brevity) at elevated temperature $T_{PLD} = 973$ K in oxygen ambience. The pressure of optically clean oxygen was 20 Pa during deposition, and it was raised to atmospheric pressure during postdeposition cooling or annealing. The thickness of the films was determined from the Laue satellites in x-ray diffraction patterns and from ellipsometric data. Cube-on-cube-type epitaxial growth of the films, with the NNO (001) planes parallel to the (001) planes of LSAT, MgO, and STO substrates and the (011) plane of DSO, was confirmed by x-ray diffraction [15]. The out-of-plane and in-plane lattice parameters, c_{film} and a_{film}, of the films on LSAT, MgO, and DSO differ from the averaged lattice parameter of the pseudocubic perovskite subcell of bulk NNO $a_{bulk} = (V_{bulk})^{1/3} \approx 3.905$ Å, where V_{bulk} is the volume of the subcell [16]. The films on LSAT, MgO, and DSO experience anisotropic lattice strain: in-plane compression and out-of-plane elongation on LSAT and in-plane expansion and out-of-plane compression on DSO and MgO. The out-of-plane

*Corresponding author: marinat@ee.oulu.fi

lattice strain $s_c = (c_{\text{film}}/a_{\text{bulk}} - 1)$ is approximately 0.66% on LSAT, −1.1% on DSO, and −0.2% on MgO.

The NNO film on STO is metrically pseudocubic with the lattice parameters close to those of the STO substrate. This similarity of the lattice parameters makes it difficult to analyze the crystal structure of the NNO/STO stack by x-ray diffraction. Here the crystal structure of the NNO film on STO was additionally studied by high-resolution transmission electron microscopy (HRTEM) on a JEOL 2200FS TEM with double Cs correctors, operated at 200 kV. To ensure stability of the NNO film during cross-sectional specimen preparation for HRTEM, samples with a thin protective layer of STO on the top of NNO were grown under conditions similar to those used for the single NNO films.

The optical properties of the NNO films and reference crystal were explored by variable-angle spectroscopic ellipsometry (VASE) using a VUV J. A. Woollam ellipsometer. The ellipsometric data were collected in a dry nitrogen atmosphere over a spectral range from 0.74 to 9.0 eV. The experimental spectra of ellipsometric angles (Δ, ψ) were extracted with an accuracy of 0.2° for Δ and 0.04° for ψ by measuring each sample at angles of incidence of 65°, 70°, and 75°. The data analysis was performed using the WVASE32 software package [17,18]. The ellipsometric spectra were fitted using a model considering a stack of semi-infinite substrate, film, surface-roughness layer, and ambient air. The optical properties of the surface-roughness layer were represented by a Bruggeman effective medium approximation [19]. We used a two-step analysis. A multioscillator model was employed to determine the initial dielectric function and layer thicknesses. The obtained thicknesses of the films were in a perfect agreement with those determined by x-ray analysis. Then the thickness was fixed, and a point-by-point fit was used to accurately extract the dielectric function for each of the films. The epitaxial films possess excellent optical homogeneity and almost atomically flat surfaces, which allowed us to obtain a mean square error (MSE) for the films in the range of 0.1–0.25, demonstrating high reliability of experimental results [20]. The dielectric functions of the substrates and the reference NNO crystal were determined using separate independent measurements. Prior to the measurements on a platelet NNO crystal with a size of approximately (5 mm × 5 mm × 1 mm), the crystal was heated to 980 K to ensure its room-temperature single-phase state [21]. The surface of the crystal was epitaxially polished.

The real and imaginary parts of the complex dielectric function, ε_1 and ε_2, were analyzed using derivative spectra. The dielectric function ($\varepsilon = \varepsilon_1 + i\varepsilon_2$) in the vicinity of a parabolic CP can be presented in the following form [10,11]:

$$\varepsilon(E) = C - A\exp(i\phi)(E - E_0 + i\Gamma)^{\gamma}, \qquad (1)$$

where the parameters are the amplitude A, phase projection factor ϕ describing the type of CP and excitonic effects, threshold energy E_0, broadening parameter Γ, and exponent γ related to the dimensionality of the CP. Here, E is the photon energy, and C is the nonresonant part of the dielectric function due to other CPs. The second derivative of the dielectric function for a two-dimensional CP is given by [12]

$$\frac{d^2\varepsilon}{dE^2} = \frac{A\exp(i\phi)}{(E - E_0 + i\Gamma)^2}. \qquad (2)$$

The derivative spectra were obtained by numerical differentiation of the dielectric functions using Origin software. Digital smoothing was performed using different filtering algorithms implemented in Origin. The selection of filtering procedure and parameters is found to affect the widths and the amplitudes of the fits based on expression (2). The energies, which are most important for our study, are less affected. For simplicity and ease of comparison between the films and the crystal, we restrict the analysis to the energies and the types of transitions assuming the phase angles to be $\phi = 0, 0.5, 1$, or $1.5\,\pi$.

III. RESULTS AND DISCUSSION

A. Epitaxial $NaNbO_3$ film on $SrTiO_3$

Due to a perfect lattice match between the pseudocubic perovskite subcell of NNO and the cubic perovskite cell of STO, pseudomorphic epitaxial growth of NNO on STO is possible. HRTEM imaging [Fig. 1(a)] and selected area electron diffraction (SAED) analysis [Fig. 1(b)] evidence the single-crystal structure of the NNO film. The epitaxial relationship between the film and the substrate is cube-on-cube type NNO(001)[100]//STO(001)[100].

As expected, the in-plane lattice parameters of NNO and STO are practically the same [Fig. 1(c)]. The in-plane lattice parameter of NNO is found to be $a_{\text{film}} = 3.905 \pm 0.008$ Å. The measured out-of-plane lattice parameter of NNO is approximately $c_{\text{film}} = 3.906 \pm 0.035$ Å [Fig. 1(d)]. The out-of-plane lattice strain in the NNO film on STO can be estimated as $s_c = (c_{\text{film}}/a_{\text{bulk}} - 1) \approx 0.02\%$. The presence of a weak lattice strain can be explained by a mismatch between the thermal expansion coefficients of NNO and STO. This mismatch leads to the development of a thermal strain when the sample

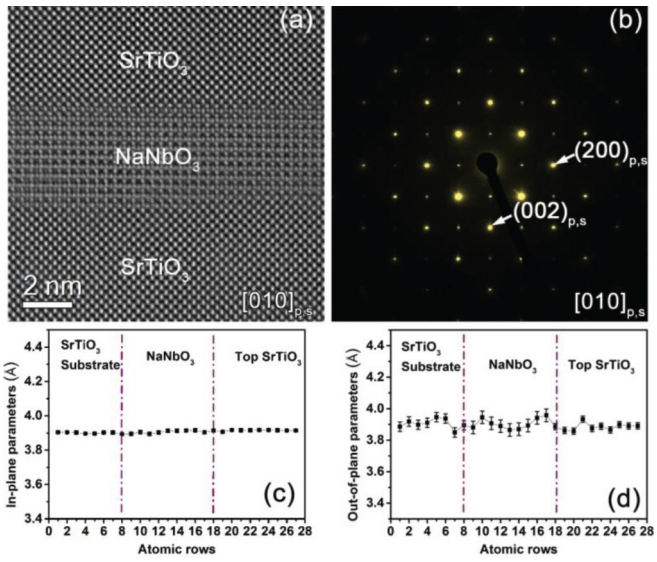

FIG. 1. (Color online) (a) Cross-sectional HRTEM image and (b) SAED pattern of the STO coated NNO/STO sample along the [010]p,s zone axis. The subscripts p and s denote the pseudocubic notation of NNO and cubic notation of STO, respectively. The mean (c) in-plane and (d) out-of-plane lattice parameters across the STO/NNO/STO stack. The error bars show the standard deviation with respect to the mean spacing along the interface in 20 atomic rows.

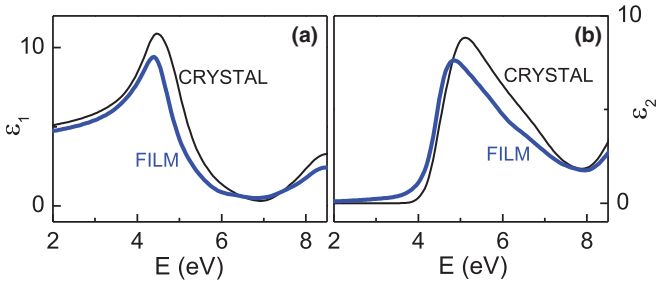

FIG. 2. (Color online) (a) Real and (b) imaginary parts of the dielectric function, ε_1 and ε_2, as a function of photon energy in the epitaxial NNO film on LSAT (thick lines) and in the NNO crystal (thin lines).

is cooled down to room temperature after high-temperature deposition.

B. Optical properties

Typical room-temperature spectra of the dielectric function are shown in Fig. 2. The spectra of ε_1 exhibit maxima at photon energies of approximately ∼4.5 eV and ∼8.5 eV, and the corresponding maxima can be seen in the spectra of ε_2 both in the films and in the crystal. The dielectric function with the two maxima agree qualitatively with those generally observed in perovskite oxide ferroelectrics [22–27]. The dielectric peaks are commonly ascribed to two groups of electronic transitions between the valence band (VB) and conduction band (CB). As long known for perovskite oxide ferroelectric crystals, the filled VB is formed mainly by oxygen $2p$ orbitals and the lowest lying empty CB derives from the transition-metal d orbitals. The d band consists of a lower energy, wide $d\varepsilon$ sub-band and a higher energy, narrower $d\gamma$ sub-band. The VB → $d\varepsilon$ and VB → $d\gamma$ transitions dominate the dielectric maxima at 4–6 eV and at 8–11 eV, correspondingly. It has been shown that the contribution of VB → $d\gamma$ transitions to the refraction index n in the visible range is larger than that of VB → $d\varepsilon$ transitions, while the linear electro-optic effect is mostly determined by polarization-induced changes in the energy and the strength of VB → $d\varepsilon$ transitions [22–25].

The dielectric maxima at ∼4.5 eV and ∼8.5 eV in the NNO films and in the crystal can thus be related to the VB → $d\varepsilon$ and VB → $d\gamma$ transitions, correspondingly. A closer inspection reveals differences between the spectra of the epitaxial films and between those of the films and the crystal. To better quantify these differences, the derivative spectra were analyzed. As an example, the derivative spectra and fits to expression (2) in the NNO crystal are shown in Fig. 3.

Derivative spectra indicate that the main contribution to the dielectric maximum at ∼4.5 eV in the NNO crystal originates from two strong CPs with energies E_0 of approximately 4.45 eV and 4.90 eV (Fig. 3). A weak CP resembling that at $E_0 = 4.9$ eV in the crystal is found in the NNO film on STO only [Fig. 4(a)]. The crystal-type CP (4.9 eV) is absent in all other films. In contrast, the strong CP, which resembles that at $E_0 = 4.45$ eV in the crystal, is seen in all spectra. The energies of this CP in the NNO films differ from 4.45 eV in the crystal.

Another important observation is related to CPs with energies of ∼8.5 eV. Compared to the NNO crystal, not

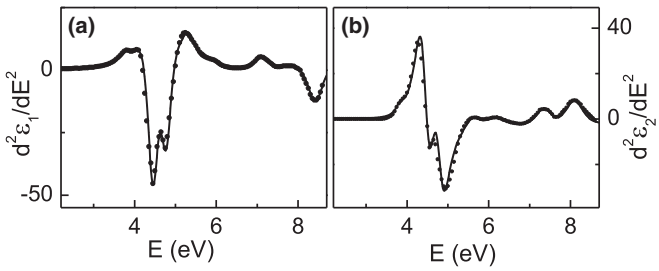

FIG. 3. Spectra of the second derivatives (a) $d^2\varepsilon_1/dE^2$ and (b) $d^2\varepsilon_2/dE^2$ in the NNO crystal.

only their energy and amplitude change in the NNO films but in some cases also their type changes. This is most clearly illustrated by the spectrum of the NNO film on DSO [Fig. 4(d)]. Finally, a moderate CP with $E_0 = 7.1$ eV in the crystal transforms into two weaker ones in the films on STO and MgO [Figs. 4(e) and 4(f)]. These new lines are very weak in the films on LSAT and DSO.

Thus, the derivative spectra demonstrate significant shifts in the energies of CPs and a suppression, splitting, or change of the type of CPs in the epitaxial NNO films compared to the NNO crystal. The obtained results point to complex changes in the band structure and interband transitions of NNO, which are induced by epitaxial growth. Compared to the NNO crystal, the epitaxial NNO films possess a different crystal structure, anisotropic lattice strain, and ferroelectric polarization [15]. All these factors may influence the interband transitions.

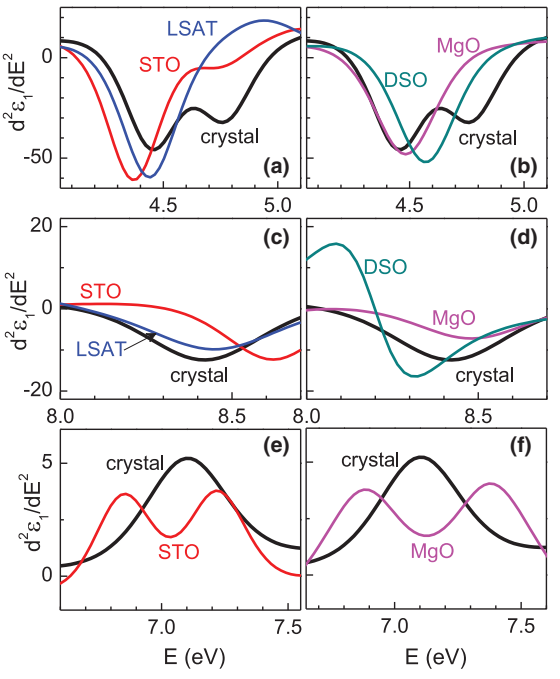

FIG. 4. (Color online) Spectra of the second derivative $d^2\varepsilon_1/dE^2$ in the vicinity of critical points at (a), (b) 4.5 eV; (c), (d) 8.5 eV; and (e), (f) 7.0 eV for the NNO films on (a), (c) STO and LSAT substrates; (b), (d) MgO and DSO substrates; (e) STO substrates; and (f) MgO substrates. The spectra of the NNO crystal are shown for comparison (thick lines).

The band structure and DOS of the cubic and the orthorhombic phases of bulk NNO have been recently calculated using first-principles methods [28,29]. In both phases, the top of the VB is formed by oxygen $2p$ orbitals. The calculated VB energies and DOS of these NNO phases are very similar [29]. The VB DOS can also be similar in the tetragonal and rhombohedral phases of NNO [9]. In contrast, the bottom of the CB in NNO is essentially set by the d orbitals of Nb. As the crystal symmetry of NNO lowers from cubic to orthorhombic, the lengths of Nb−O bonds change, and the angles of O-Nb-O bonds deviate from 90°. This leads to a lower CB energy in cubic NNO compared to orthorhombic NNO [29]. Besides, the CB energy can red shift when the crystal structure changes from rhombohedral to tetragonal [9]. Thus, it seems that changes in crystal symmetry do not affect the VB, but they can strongly influence the bottom of the CB. Moreover, crystal phases with higher structural symmetry may have a CB at lower energy.

According to our previous thermo-optical studies [15], cube-on-cube-type epitaxial NNO films are in the ferroelectric state. First-principles theoretical phase diagram suggests that this state corresponds to the r phase, whose crystal symmetry is higher than that of bulk orthorhombic NNO [30]. Theoretical calculations of the band structure and DOS for the r phase have not been reported so far. Considering the above described theoretical results, one may expect a lowering of the CB energy in the NNO films compared to the NNO crystal due to changes in crystal symmetry. Additionally, the NNO films experience epitaxial lattice strain. Strain is also known to lower the CB energy [6–9]. Thus both the change in crystal symmetry and the presence of lattice strain should induce red shifts in the dielectric spectra of the NNO films. In the following, we analyze the energies of the strongest CPs (at ∼4.5 eV and ∼8.5 eV) in order to verify the discussed theoretical conclusions.

The energies of the two selected CPs do not demonstrate an obvious tendency in the r-type films compared to the orthorhombic crystal [Fig. 5(a)]. Considering that the NNO film on STO is practically free of lattice strain, the role of crystal symmetry can be evaluated by focusing on this film first. Compared to the NNO crystal, the NNO film on STO exhibits a red shift of the CP at ∼4.5 eV, which agrees with theoretical predictions. However, a simultaneous strong blue shift of the CP at ∼8.5 eV opposes theory. In addition to this controversial behavior of the two CPs, suppression and splitting of other CPs also takes place (Fig. 4). Thus, the theoretically calculated red shift of the CB DOS for crystals with higher structural symmetry is insufficient for explaining the changes in the NNO film on STO compared to the crystal. It is worth noting here that the NNO film on STO possesses ferroelectric polarization [15], whose influence on the CB DOS is difficult to model [8].

In order to evaluate the effect of lattice strain on CPs, the energies and amplitudes of the two CPs (at ∼4.5 eV and at ∼8.5 eV) are analyzed as a function of strain in the r-type NNO films on different substrates. The NNO film on the STO substrate is taken as a reference because of negligible strain therein. According to theoretical calculations [8], anisotropic lattice strain can lower the CB energy in epitaxial paraelectric films. Correspondingly, with increasing strain s_c, the energies

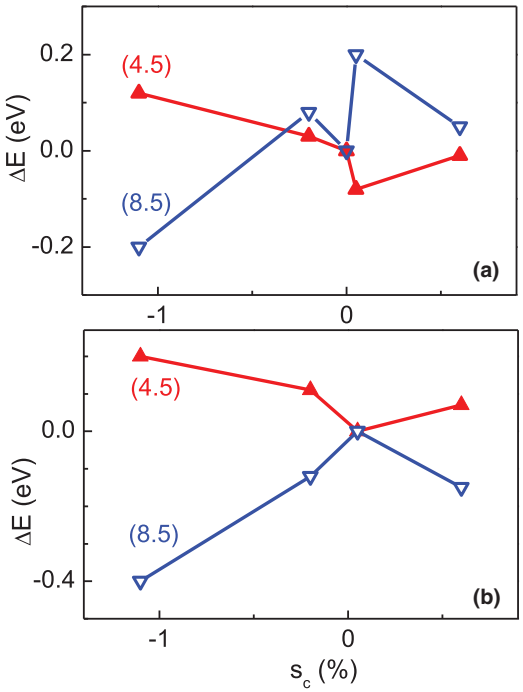

FIG. 5. (Color online) Relative changes of the energy ΔE of the critical points at approximately 4.5 and 8.5 eV as a function of the out-of-plane lattice strain in the NNO films (a) compared to the crystal and (b) compared to the NNO film on STO.

of the CPs should red shift in the NNO films. Consistent with these theoretical predictions, the higher energy CP at ∼8.5 eV red shifts with increasing magnitude of s_c [Fig. 5(b)]. However, the CP at ∼4.5 eV shows an opposite behavior: it blue shifts with increasing magnitude of s_c [Fig. 5(b)]. Again it should be stressed that the NNO films are ferroelectric [15]. Hence, the theoretical calculations made for the paraelectric phase are not directly applicable here. As shown using different theoretical methods, ferroelectric polarization can raise the CB energy [8,25,26]. The VB–CB energy separation can increase with increasing ferroelectric polarization. This suggests a blue shift of the CPs. Importantly, ferroelectric polarization can be enhanced (or induced) in epitaxially strained films due to strain–polarization coupling in perovskite ferroelectrics [31,32]. This is the case in the studied NNO films [15]. With increasing lattice strain, the polarization increases, and, consequently, the CPs should blue shift. Based on these insights, the blue shift of the lower energy CP at ∼4.5 eV in the epitaxial NNO films [Fig. 5(b)] can be attributed to the dominating effect of ferroelectric polarization, while the behavior of the CP at ∼8.5 eV seems to be sensitive to lattice strain but not to ferroelectric polarization. Interestingly, this lack of sensitivity of the higher energy CPs to polarization agrees with experimental observations in many perovskite oxide ferroelectric crystals. The crystal polarization is known to raise the energy of the lower energy VB → $d\varepsilon$ transitions with little or no influence on the higher energy VB → $d\gamma$ transitions [22,24,25].

The apparent polarization-independent behavior of the CP at ∼8.5 eV may be ascribed to effects of polarization other than the rise of the CB energy. In particular, polarization can

produce splitting of energy levels and CPs [26]. The change of type of CP at ∼8.5 eV in the NNO film on DSO [Fig. 4(d)] may be considered as an indication of this effect. Also, the presence of two CPs at ∼7 eV separated by 0.3–0.5 eV in the ferroelectric NNO films compared to the CP at 7.1 eV in the nonferroelectric crystal may point to a polarization-induced splitting. More extensive theoretical and experimental studies are required to further clarify the impact of ferroelectric polarization on band structure and interband transitions in perovskite oxide ferroelectrics.

As shown here, the energies of interband transitions in epitaxial ferroelectric films can be tuned by controlling the crystal structure, lattice strain, and ferroelectric polarization therein. Besides the energy shifts, significant changes in amplitudes, numbers, and types of CPs are found in the epitaxial NNO films compared to the NNO crystal and as a function of lattice strain. This implies that effects of epitaxy are more complex than a simple increase or decrease of band energies. Importantly, ferroelectric polarization plays a more critical role than usually assumed. Long-range ferroelectric polarization can affect the energies and also the splitting and degeneracy of band levels. Correspondingly, the optical properties of epitaxial ferroelectric films can be strongly influenced by variations of polarization, which in turn are correlated to changes in lattice symmetry and/or strain. A better knowledge and understanding of effects of epitaxy on the band structure and electronic transitions in perovskite oxide ferroelectrics can have a significant impact on development of advanced optoelectronic materials.

IV. CONCLUSIONS

We analyzed the interband transitions in cube-on-cube-type epitaxial ferroelectric NNO films on different substrates using VASE in the spectral range of 0.74–9 eV. Accurate second derivative analyses of the dielectric functions indicate that the energies, amplitudes, and number of CPs in the films differ significantly from those of a NNO reference crystal. The differences are explained by epitaxially induced changes of crystal symmetry, lattice strain, and strain-enhanced ferroelectric polarization in the films. It is suggested that the energies, splitting, and degeneracy of band levels are strongly influenced by ferroelectric polarization in the NNO films. Such variations of ferroelectric polarization, either caused by changes in lattice symmetry and/or strain, may be used to tailor the optical properties of epitaxial films in photonic and optoelectronic devices.

ACKNOWLEDGMENTS

The authors acknowledge support from the Academy of Finland (Grants No. 260361 and No. 264961), Grant Agency of Czech Republic (Grants No. 15–13778S and No. 15–15123S), the Finnish Funding Agency for Innovation (Grant No. 400.31.2013), and the European Research Council (ERC-2012-StG 307502-E-CONTROL). TEM analysis was conducted at the Aalto University Nanomicroscopy Center (Aalto-NMC).

[1] B. W. Wessels, Annu. Rev. Mater. Res. **37**, 659 (2007).
[2] M. Qin, K. Yao, and Y. C. Liang, Appl. Phys. Lett. **93**, 122904 (2008).
[3] R. Guo, L. You, Y. Zhou, Z. S. Lim, X. Zou, L. Chen, R. Ramesh, and J. Wang, Nat. Commun. **4**, 1990 (2013).
[4] M. J. Dicken, L. A. Sweatlock, D. Pacifici, H. J. Lezec, K. Bhattacharya, and H. A. Atwater, Nano Lett. **8**, 4048 (2008).
[5] S. Abel, T. Stöferle, C. Marchiori, C. Rossel, M. D. Rossell, R. Erni, D. Caimi, M. Sousa, A. Chelnokov, B. J. Offrein, and J. Fompeyrine, Nat. Commun. **4**, 1671 (2013).
[6] J. Singh, *Electronic and Optoelectronic Properties of Semiconductor Structures* (Cambridge University Press, New York, 2003).
[7] A. Walsh, C. R. A. Catlow, K. H. L. Zhang, and R. G. Egdell, Phys. Rev. B **83**, 161202 (2011).
[8] R. F. Berger, C. J. Fennie, and J. B. Neaton, Phys. Rev. Lett. **107**, 146804 (2011).
[9] F. Wang, I. Grinberg, and A. M. Rappe, Appl. Phys. Lett. **104**, 152903 (2014).
[10] M. L. Cohen and J. R. Chelikowsky, *Electronic Structure and Optical Properties of Semiconductors* (Springer-Verlag, Heidelberg, 1989).
[11] P. Yu and M. Cardona, *Fundamentals of Semiconductors* (Springer-Verlag, New York, 1996).
[12] G. E. Jellison, Jr., I. Paulauskas, L. A. Boatner, and D. J. Singh, Phys. Rev. B **74**, 155130 (2006).
[13] S. G. Choi, A. M. Dattelbaum, S. T. Picraux, S. K. Srivastava, and C. J. Palmstrøm, J. Vac. Sci. Technol. B **26**, 1718 (2008).
[14] M. Rossle, C. N. Wang, P. Marsik, M. Yazdi-Rizi, K. W. Kim, A. Dubroka, I. Marozau, C. W. Schneider, J. Humlicek, D. Baeriswyl, and C. Bernhard, Phys. Rev. B **88**, 104110 (2013).
[15] M. Tyunina, D. Chvostova, O. Pacherova, T. Kocourek, M. Jelinek, L. Jastrabik, and A. Dejneka, Sci. Technol. Adv. Mater. **15**, 045001 (2014).
[16] C. N. W. Darlington and K. S. Knight, Physica B **266**, 368 (1999).
[17] *Guide to Using WVASE 32: Spectroscopic Ellipsometry Data Acquisition and Analysis Software* (J. A. Woollam Inc., Lincoln, Nebraska, 2008).
[18] J. A. Woollam, J. N. Hilfiker, T. E. Tiwald, C. L. Bungay, R. A. Synowicki, D. E. Meyer, C. M. Herzinger, G. L. Pfeiffer, G. T. Cooney, and S. E. Green, Proc. SPIE **4099**, 197 (2000).
[19] H. Fujiwara, J. Koh, P. I. Rovira, and R. W. Collins, Phys. Rev. B **61**, 10832 (2000).
[20] B. Johs and C. M. Herzinger, Quantifying the accuracy of ellipsometer systems, Phys. Stat. Sol. (c) **5**, 1031 (2008).
[21] M. Tyunina, A. Dejneka, D. Rytz, I. Gregora, F. Borodavka, M. Vondracek, and J. Honolka, J. Phys.: Condens. Matter **26**, 125901 (2014).
[22] M. DiDomenico, Jr. and S. H. Wemple, J. Appl. Phys. **40**, 720 (1969).
[23] S. H. Wemple and M. DiDomenico, Jr., J. Appl. Phys. **40**, 735 (1969).

[24] N. Uchida, J. Appl. Phys. **44**, 2072 (1973).
[25] L. Castet-Mejean and F. M. Michel-Calendini, Phys. Rev. B **23**, 1 (1981).
[26] J. R. Brews, Phys. Rev. Lett. **18**, 662 (1967).
[27] E. Wiesendanger, Ferroelectrics **6**, 263 (1973).
[28] G. Liu, S. Ji, L.Yin, G. Xu, G. Fei, and C. Ye, J. Appl. Phys. **109**, 063103 (2011).
[29] P. Li, S. Ouyang, G. Xi, T. Kako, and J. Ye, J. Phys. Chem. C **116**, 7621 (2012).
[30] O. Diéguez, K. M. Rabe, and D. Vanderbilt, Phys. Rev. B **72**, 144101 (2005).
[31] N. A. Pertsev, A. G. Zembilgotov, and A. K. Tagantsev, Phys. Rev. Lett. **80**, 1988 (1998).
[32] C. Ederer and N. A. Spaldin, Phys. Rev. Lett. **95**, 257601 (2005).